Online Monitoring of the Evolution of Polyelectrolyte Characteristics during Postpolymerization Modification Processes

Ahmet Paril,[‡] Alina M. Alb,[†] and Wayne F. Reed*,[†]

Physics Department, Tulane University, New Orleans, Louisiana 70118, and Faculty of Sciences & Letters, Istanbul Technical University, 34469 Maslak, Istanbul, Turkey

Received February 2, 2007

Revised Manuscript Received May 14, 2007

Introduction. Postpolymerization modification is an important approach to generating advanced materials from known polymerization methods and is widespread in research and industrial production. Improvements in the efficiencies and selectivities of postpolymerization reactions have resulted in the ability to prepare materials with tailored degrees of functionality being attached to the polymer backbone after the starting polymer has been produced.

Many postpolymerization chemical transformations are used, such as grafting, hydrolysis of pendant esters, activated esters, nitrile and amides, quaternization of pendant amines, sulfonation of aromatic units, and the growing use of the Huisgen "click" reaction,[1] whose power and versatility have been amply demonstrated.[2−4]

Characterization is generally only performed at the end of such modification reactions, with little if any real-time data on the extent of reaction available. Comprehensive online monitoring of these processes has not yet been demonstrated, and success in this area will greatly increase the opportunities for new materials. It is hence the object of this work to demonstrate the feasibility of monitoring changes in polymer properties while a modification reaction is occurring. Automatic continuous online monitoring of polymerization reactions (ACOMP) is used for this. ACOMP theory and practice have been adequately described previously.[5,6]

For this demonstration the base hydrolysis of polyacrylamide (Paam) was chosen. The reaction gradually converts the neutral polyacrylamide into a copolymer with an increasing proportion of charged monomers bearing carboxylate groups. The ACOMP method is not limited to such modifications. In fact, it will be applicable wherever a measurable signal corresponding to a chemical or physical change can be measured in the flowing sample stream. Detectors such as ultraviolet/visible spectrophotometers, fluorimeters, FTIR, etc., can be used, in addition to the light scattering, viscosity, conductivity, and refractometric detectors used in this work.

Materials and Methods. Paam was synthesized via free radical polymerization and was used for the hydrolysis reactions whose reaction and detection conditions are given in Table 1. Gel permeation chromatography (GPC) measurements and separate batch measurements yielded $M_w = 950\,000$ g/mol for the starting Paam, and GPC polydispersity was near the expected ratios of 3:2:1 for M_z:M_w:M_n. No detectable degradation of the Paam occurred during hydrolysis, as verified by additional independent GPC measurements on end products. Also listed in Table 1 are separate potentiometric titration measurements for the final conversion values of some of the end products.

ACOMP was utilized as previously described. In this work a two-pump arrangement with high-pressure mixing was used. The detector train comprised a Brookhaven Instruments BI-MwA multiangle light scattering detector, a custom-built viscometer, and a Shimadzu refractive index detector. Additionally, a conductance probe was inserted into the reactor and provided an additional monitored signal.

An aqueous dilution solvent of moderate ionic strength (IS) in the range of 0.025−0.050 M was generally used. This moderate IS allowed the evolution of the polyelectrolyte characteristics of the polymer to be monitored. If high IS were used, the polyelectrolyte effects would be suppressed and not measurable. If extremely low IS were used, then "strong" polyelectrolyte effects would hamper the interpretation of the data. "Strong" polyelectrolyte effects refer to those commonly reported at extremely low ionic strength. One such is the electroviscous effect, whereby reduced viscosity η_r increases as a polyelectrolyte solution is diluted with a fixed IS solvent (an example of which is given below).[7,8] Another effect involves strong interparticle correlations leading to an angular maximum in scattered light.[9−13] While it would be interesting in a separate study to watch such effects build in, and hence monitor their evolution as a function of linear charge density ξ, such effects are not pursued here in favor of establishing a more practical approach to monitoring polymer modifications.

Results and Discussion. Raw ACOMP data are shown in Figure 1 (reaction 2). IS in the detector train was 0.028 M. Reduced viscosity η_r increases 4-fold during the reaction. Simultaneously, the light scattering (LS) decreases due to the increase in electrostatically enhanced A_2 and A_3. This effect is strong enough to drive LS back into the solvent level. The effect on LS is often greater than on viscosity because the excluded volume controlling A_2 and A_3 is enhanced by ξ due to both an increase in coil dimensions (which, under nondraining conditions, parallels the increase in η_r) and the electrostatic field around the polyelectrolyte, which further increases excluded volume but has no effect on hydrodynamic dimensions and the polymers' motion through the solvent.[14] The conductivity σ decreases during the reaction as OH^- is consumed and COO^-groups are formed along the polymer chains.

The raw viscosity, LS, and σ data contain extensive information on the evolution of the polyelectrolyte properties during hydrolysis. Some associated phenomena can be described without models, but others require model-dependent interpretation. Qualitative effects of increasing ξ are immediately apparent in the raw viscosity and LS data. η_r is computed directly from raw viscosity data with no models or calibration factors needed, since

$$\eta_r(t) = \frac{V(t) - V_s}{c_p V_s} \tag{1}$$

where $V(t)$ is the raw voltage at any time t, c_p is the polymer concentration in g/cm^3 (which remains constant during the hydrolysis experiment), and V_s is the baseline viscosity signal for the pure solvent.

At the values of c_p and IS in the detector η_r is very close to intrinsic viscosity $[\eta]$. This is illustrated in Figure 2 for the end product of experiment 5, where ACM (automatic continuous

* Corresponding author. E-mail: wreed@tulane.edu.
† Tulane University.
‡ Istanbul Technical University.

10.1021/ma070291x CCC: $37.00
Published on Web 05/27/2007

Table 1. Experimental Conditions[a]

		$C_{reactor}$			$C_{detector\ train}$	
expt no.	end product conversion by potentiometric titration	C_{Paam} (M)	C_{NaOH} (M)	T (°C)	C_{Paam} (M)	IS (M)
1	49%	0.2322	0.05	60	0.016	0.009
2	not available	0.1160	0.1	35	0.016	0.028
3	not available	0.1159	0.1	60	0.016	0.028
4	46%	0.1160	0.1	60	0.0074	0.054
5	40%	0.1162	0.1	35	0.0074	0.054

[a] NaCl concentration in reactor was 0.010 M for all experiments.

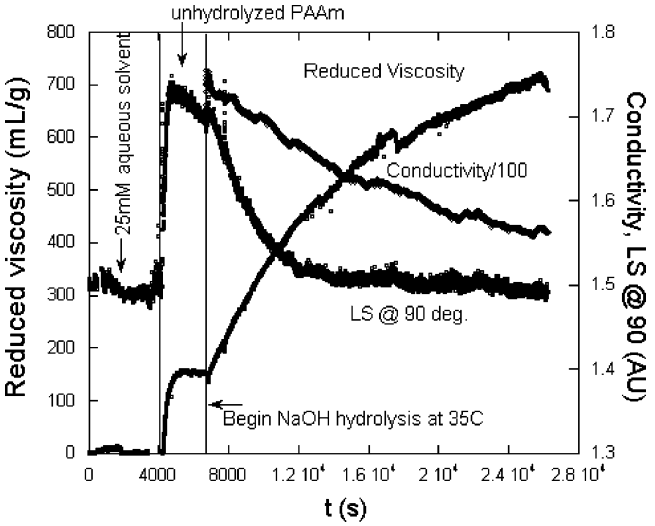

Figure 1. Raw ACOMP data for LS (only 90° shown) and σ for reaction 2, including η_r, calculable from eq 1 with no calibration or model assumptions.

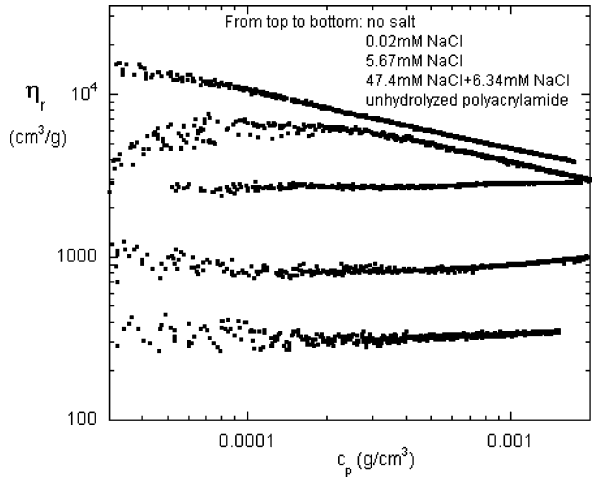

Figure 2. η_r vs c_p at various IS. The electroviscous effect appears in pure water and at very low ionic strength (0.000 02 M).

mixing) was used to ramp c_p from 0.002 g/cm^3 to 0 at fixed IS. It is readily seen that at the concentrations in the detector train η_r is very close to $[\eta]$. The c_p ramp data in Figure 2 are shown for IS of around 5 and 50 mM, with the expected results that $[\eta]$ is markedly lower at higher IS. The hydrodynamic parameter κ_H in the expansion $\eta_r = [\eta] + \kappa_H[\eta]^2$ is found to be 0.018 and 0.18 respectively for the IS 0.005 and 0.05 M cases (lower two curves) in Figure 2. This yields less than 5% error by taking $[\eta] \sim \eta_r$ in the first case and less than 10% in the latter case. A ramp of unhydrolyzed Paam is also shown in the figure, with the expected result that $[\eta]$ is less than for the hydrolyzed material.

Also shown for contrast in Figure 2 are ramps of c_p at very low ionic strength, 0.000 02 M, and with pure water. The striking electroviscous effect mentioned above is readily apparent for these two cases. Clearly, serious errors would result if $[\eta]$ were assumed simply to be equal to η_r at finite c_p. At $c_p = 0.001$ g/cm^3, for example, the error would be several hundred percent.

$[\eta]$, closely approximated by the directly measured η_r, then yields effective polymer viscometric volume V_H (for an equivalent sphere). Computational expressions for $[\eta]$ can be obtained starting with the Flory relation

$$[\eta]_0 = \frac{\Phi(\sqrt{6}\langle S^2\rangle_0^{1/2})^3}{M} \tag{2}$$

where $\Phi = 2.56 \times 10^{23}$ M^{-1} and molar mass M is known from separate model-independent measurements. Equation 2 applies to the case of non-free-draining and no intrachain excluded volume considerations, and $\langle S^2\rangle_0$ is the unperturbed mean-square radius of gyration. The use of $[\eta]_0$ in eq 2 instead of $[\eta]$ denotes the fact that excluded volume is not taken into account. One way of then taking excluded volume into account is by applying a viscometric expansion factor to $[\eta]_0$, as is discussed briefly below.

There is clearly a correlation between increasing $[\eta]$ and ξ, but the relationship requires a model. ξ, in turn, is proportional to the fractional degree of hydrolysis δ (fraction of acrylamide monomers hydrolyzed) without any assumptions, as long as ξ is well below the "counterion condensation threshold".[15]

$\delta(t)$ is an important practical characteristic to monitor since it allows running the reaction to any degree of conversion desired. In the current data there is no model-independent route to obtaining conversion, in contrast to normal ACOMP measurements of polymerization reactions, where model-independent conversion is immediately obtained from the raw data. This suggests that future studies use a chemically specific detector, such as FTIR, for direct measurement of conversion.

What follows, nonetheless, is a first attempt to relate $\sigma(t)$ to $\delta(t)$. Below the CC threshold ξ tracks $\delta(t)$ via l_B and monomer contour length b.

$$\xi(t) = \frac{l_B\delta(t)}{b} \tag{3}$$

The task here is to solve for the time dependence of the accumulation of COO^- groups on the hydrolyzing chain, which well below the CC threshold yields the average linear charge density, and then use an approximate model to relate the decrease of $\sigma(t)$ caused by the loss of conductivity due to the loss of free OH^- and the correspondingly smaller increase in conductivity due to the increasing ξ as COO^- groups accumulate on the chains.

For each Am monomer converted to COO^- an OH^- is lost

$$\frac{d[Am]}{dt} = -\frac{d[COO^-]}{dt} = \frac{d[OH^-]}{dt} = -k[OH^-][Am] \tag{4}$$

Solving this allows [Am] to be computed and, with a model for the relationship between the experimentally measured decrease of $\sigma(t)$ due to loss of OH^- and the buildup of charge groups on the polymer, $\delta(t)$ can be computed. This first approach holds up to approximately $\delta(t) \sim 0.35$, where counterion condensation commences in the most naive counterion condensation model.

Equation 4 leads to a single second-order, nonlinear differential equation in $[OH^-]$

$$\frac{d^2[OH^-]}{dt^2} - \frac{1}{[OH^-]}\left\{\frac{d[OH^-]}{dt}\right\}^2 + k[OH^-]\frac{d[OH^-]}{dt} = 0 \quad (5)$$

and an identical equation for [Am], with initial values of $[OH^-](0)$ and [Am](0), respectively, whose solutions are

$$[OH^-](t) = [OH^-](0) \times \left\{\frac{1 - [Am](0)/[OH^-](0)}{1 - ([Am](0)/[OH^-](0))\exp[-([OH](0) - [Am](0))kt]}\right\} \quad (6)$$

and

$$[Am](t) = [Am](0) \times \left\{\frac{1 - [OH^-](0)/[Am](0)}{1 - ([OH^-](0)/[Am](0))\exp[-([Am](0) - [OH^-](0))kt]}\right\} \quad (7)$$

The concentration of COO^- groups building up on the polymer is given by

$$[COO^-](t) = \{[Am](0) - [Am](t)\} \quad (8)$$

The fractional conversion is given by

$$\delta(t) = \frac{[Am](0) - [Am](t)}{[Am](0)} \quad (9)$$

A model is now needed to connect $\sigma(t)$ to $\delta(t)$. The following model is not claimed to be definitive but is a reasonable starting point before considering more refined approaches that take into account numerous possible effects.

Let σ_0 be the portion of the total reactor conductivity σ due to any added salt, e.g., the NaCl shown in Table 1. That is, σ_0 is constant and is the sum of the conductivity due to $[Na^+]$ and $[Cl^-]$, where $[Na^+] = [Cl^-] = [NaCl]$. The remaining solution conductivity $\Delta\sigma = \sigma - \sigma_0$ is then due to (1) the additional Na^+ ions from the NaOH, whose concentration $[Na^+]_{NaOH}$ is unchanging as long as there is no counterion condensation, (2) $[OH^-]$, which diminishes as hydrolysis proceeds, and (3) the contribution to the hydrolyzing Paam whose molar conductivity in $(\Omega\ cm\ mol)^{-1}$ increases with the chains' increasing linear charge density ξ, while the total concentration of chains' [Paam] remains constant and equal to the initial amount $[Paam]_0$. $[Paam]_0 = [Am]_0/N$, where N is the average degree of polymerization, which does not change during hydrolysis, as verified by GPC measurements made on hydrolysis reaction aliquots. Polydispersity is ignored in this first approach. The molar conductivity for each of these terms is denoted as Σ_{Na^+}, Σ_{OH^-}, and $\Sigma_{p^-}(t)$, where the subscript p^- indicates the anionic polyelectrolyte formed by the hydrolysis, and its time dependence indicates it changes in time as ξ increases.

$$\Delta\sigma(t) = [Na^+]_{NaOH}\Sigma_{Na^+} + [OH^-](t)\Sigma_{OH^-} + [Paam]_0\Sigma_{p^-}(t) \quad (10)$$

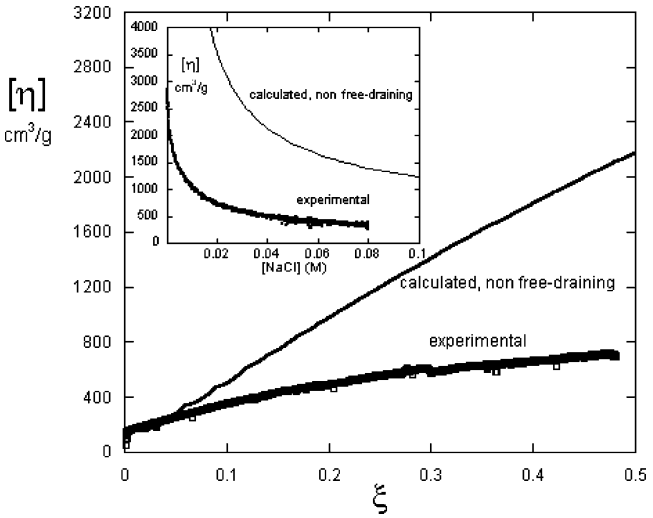

Figure 3. Evidence for deviation from non-free-draining; the experimental values are consistently below computed values for non-free-draining, using combined EPL/EEV theories. The main figure is measured and computed $[\eta]$ vs ξ, during hydrolysis experiment 5. ξ for the experiment was obtained using eqs 3−12. The inset is measured and computed $[\eta]$ vs [NaCl] for the end product of experiment 5, for which $\xi = 1$.

Concentrating on the origin of $\Sigma_{p^-}(t)$, consider the polyanion drifting at terminal velocity v in an electric field E. The microscopic form of Ohm's law is $J_{p^-} = \sigma_{p^-}E$, where J_{p^-} is current density due to the polyanion drift in E and $\sigma_{p^-}(t) = \Sigma_{p^-}(t)[Paam]$-(0) is the polyanion conductivity. By definition $J_{p^-} = \rho_{p^-}v$, where ρ_{p^-} is the solution volume charge density due to the polyanion. The magnitude of the electrical force on the polyanion, ignoring any screening and counterion condensation effects, is $F_E = ZeE$, where Z is the number of elementary charges on a polyanion. In this approximation $\rho_{p^-}(t) = Ze[Paam](0)N_A$, where N_A is Avogadro's number. At terminal or drift velocity v, F_E is balanced by the drag force $F_D = fv$, where f is the polyanion frictional factor. In the nondraining limit $f = 6\pi\eta R_H$, where η is the pure solvent viscosity and R_H is the equivalent hydrodynamic radius, which is proportional to $[\eta]^{1/3}$. Combining these terms yields

$$\Sigma_{p^-}(t) = \frac{(\delta(t)N)^2}{6\pi\eta R_H} \quad (11)$$

It was recently demonstrated that at the concentrations of Paam used in this type of hydrolysis the solution viscosity due to the polyelectrolyte itself does not appreciably affect ionic conductivities, so that η = constant. Although R_H varies, it varies only as $[\eta]^{1/3}$, so that R_H increases very slowly as hydrolysis proceeds and is taken as constant in the first approximation. This leads to

$$\Delta\sigma(t) = [Na^+]_{NaOH}\Sigma_{Na^+} + [OH^-](t)\Sigma_{OH^-}\beta\delta(t)^2 \quad (12)$$

β includes all the constants in eq 12. Four adjustable parameters, the constant first term on the right-hand side, Σ_{OH^-}, β, and the rate constant k, are then used to fit the conductivity data, using the functional forms for $[OH^-]$ and $\delta(t)$ from the above analysis. $\delta(t)$ can then be computed from the best fit value of k. This procedure was used to relate $\Delta\sigma(t)$ to $\delta(t)$ and hence to ξ (for $\xi < 1$) using eq 2.

Figure 3 shows $[\eta]$ vs ξ, where ξ was determined according to the above procedure. It is approximately linear at very low values of ξ but then has a negative second derivative after about $\xi = 0.1$. This effect has been measured by others for partially

hydrolyzed Paam[16−18] including Zema and Kowblansky,[19] who used several samples of partially hydrolyzed Paam. Their conclusion was that the effect was due to much broader and extensive counterion condensation than the naive theory predicts, leading to less coil expansion than expected.

While there is good experimental and computational evidence that counterion condensation does not have a sharp threshold, it seems there may be other, larger effects behind the nonlinearity. In fact, if computations of mean-square radius of gyration $\langle S^2\rangle$ are made using a well-established combination of electrostatic persistence length (EPL) and electrostatic excluded volume (EEV),[20,21] based on the original theories by Odijk[22,23] and Skolnick and Fixman,[24] *with no adjustable parameters*, then there is an *approximate* linear proportionality between $[\eta]$ and ξ, when $[\eta]$ is computed on the basis of non-free-draining (sometimes also referred to simply as "nondraining"). The computational procedure involves first calculating the electrostatic persistence length, whence the unperturbed $\langle S^2\rangle_0$ is found in the wormlike chain model, after which the static expansion factor α_s based on electrostatic excluded volume effects is computed, and the full value of $\langle S^2\rangle$ is found via $\langle S^2\rangle = \alpha_s^2 \langle S^2\rangle_0$. $[\eta]_0$ is then computed via eq 2, and the full value of $[\eta]$ is computed via $[\eta] = \alpha_h^3[\eta]_0$, where α_h is the viscometric expansion factor.

The fact that the experimental $[\eta]$ falls below the computed one based on EPL/EEV and non-free-draining (eq 2) is strong evidence for deviations from the nondraining assumption; i.e., as the coil opens up, there is more and more draining through the coil. The computed value of $[\eta]$ is shown in Figure 3, and it is clearly much higher than the experimental values. In the curve the approximation was made that $\alpha_h = \alpha_s$.

A similar effect was also noted in ref 16 and for other polymers such as sodium hyaluronate,[25] wherein the self-diffusion coefficient, obtained by extrapolation to $c_p = 0$ and $q = 0$ of mutual diffusion coefficients from dynamic light scattering, did not vary strongly with ionic strength, whereas $\langle S^2\rangle$ was strongly dependent on IS. In fact, the $\langle S^2\rangle$ vs IS behavior computed, without adjustable parameters, from the EPL/EEV theory matched the experimental values obtained by the static light scattering angular envelope very well.

Further evidence for deviations from non-free-draining are seen in the inset to Figure 3. In this, the same end product from experiment 5 was ramped at 0.0013 g/cm^3 vs [NaCl], and $[\eta]$, closely approximated by η_r, is shown. While there is a large decrease in η_r with IS, it is much less than predicted by EPL/EEV and non-free-draining. In fact, even taking into account that α_h can be less than α_s, the predicted values of $[\eta]$ are still much higher than the experimental values. In the Figure 3 inset $[\eta]_0$ was again computed with eq 2, with the EPL model alone for $\langle S^2\rangle_0$, and the viscosity expansion factor α_h was then related this time to α_s (from the EPL/EEV treatment) using the Kurata−Yamakawa semiempirical expression[26]

$$\alpha_\eta^{\ 3} = \alpha_s^{\ 2.43} \tag{13}$$

This yields a computed $[\eta] = \alpha_s^{2.43}[\eta]_0$, which is less than found by use of the Flory equation and the perturbed values of $\langle S^2\rangle$ computed by $[\eta] = \alpha_s^3[\eta]_0$, but these values are still far higher than the experimental ones.

Hence, there is good evidence for deviations from non-free-draining, which is interesting from the point of view of polymer physics but also has the unfortunate effect that monitoring η_r does not provide a route to computing ξ. Nonetheless, the monitored η_r itself can be a very useful index of how far the hydrolysis has gone in conferring desired intrinsic viscosity characteristics on the end product.

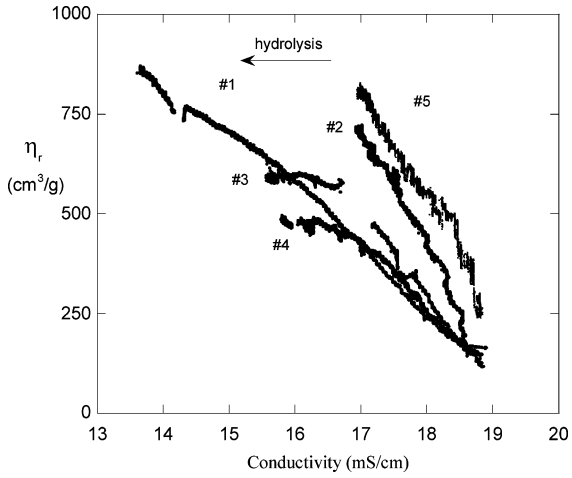

Figure 4. η_r vs σ for the experiments in Table 1.

Figure 4 shows η_r vs σ for all the experiments. The significantly different initial slopes of experiments 2 and 5 reflect the fact those hydrolyzes were carried out at $T = 35$ °C, where the conductivities are lower than at 60 °C. Other differences among the curves are due to factors that include Paam concentration and IS in the reactor and the detector train. Results from experiments 1, 3, and 4 show strong decreases in the slope as the reaction proceeds (i.e., from high to low conductivity), and experiments 3 and 4 arrive at a plateau, even though σ continues to decrease; i.e., although further COO^- groups are formed on the polymer (consuming additional free $OH^-$and lowering σ), $[\eta]$ stops increasing. The two most likely origins of the effect include both deviations from non-free-draining, and counterion condensation. In this latter ξ ceases to change despite increasing stoichiometric charge on the chain so that there is no more swelling of the coil. For a contour monomer length of $b = 0.256$ nm, $\xi = 1$ at $\delta = 0.36$.[27] The approach to the plateaus in experiments 3 and 4 is gradual; i.e., nothing suggests a sharp transition at $\xi = 1$. The lack of a sharp transition has been found in more elaborate models for counterion condensation that take chain and counterion entropy and other effects into account.[28] At this point, however, it is not possible to unambiguously separate out how much of the decrease in slope in Figure 4 is due to counterion condensation and how much to deviations from non-free-draining.

The LS data readily provide evidence of increasing ξ, but analysis is difficult due to the interplay of intra- and interparticle interference effects on the angular scattering envelope. The relation between excess scattering $I_R(q,c)$ and the single particle form factor $P(q)$ and interparticle structure factor $S(q)$ is

$$\frac{I_R(q)}{K} = Mc_pS(q)\,P(q) \tag{14}$$

When interparticle interference is negligible, $P(q)$ is the dominant effect and the slope $d[Kc_p/I_R(q)]/dq^2$ equals $\langle S^2\rangle_z/3M_w$ for $q^2\langle S^2\rangle_z \ll 1$. Figure 5 shows this slope for experiment 5. At the beginning the interactions of the neutral polymer have negligible effect on the slope (as confirmed by separate experiments on neutral Paam), but as the polymer becomes weakly charged this slope increases reflecting the increased $\langle S^2\rangle$ as the coil swells. As the coil size and the electrostatic interactions get larger as hydrolysis proceeds and ξ increases, interparticle interactions become important and $S(q)$ becomes dominant. It is well-known that this leads to a decrease in the

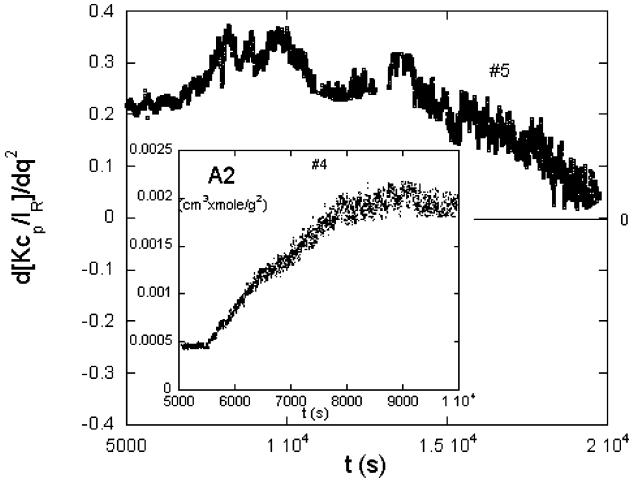

Figure 5. $d[kc_p/I(q)]/dq^2$ for experiment 5. The inset is A_2 for experiment 4.

slope, which is seen in Figure 5 after about 10 000 s. When the interparticle correlations become strong enough, there usually appears a maximum in $S(q)$, which leads to a decreasing $Kc_p/I_R(q)$ vs q before the maximum; i.e., a negative slope appears at low q. The position of the $S(q)$ maximum that shifts to higher q as c_p increases, further increasing the magnitude of the negative slope, $d[Kc_p/I_R(q)]/dq^2$.

The inset to Figure 5 gives an example of how A_2 increases as hydrolysis proceeds (experiment 4, 0.054 M = IS).

Conclusions. The ACOMP approach demonstrates that physical properties of polymers can be monitored during modification reactions. In the particular example here, physical properties due to the increasing polyelectrolyte nature of the hydrolyzing polymer were measured during the modification reactions. As is often the case with polyelectrolyte solutions, several simultaneous effects lead to difficulties in interpreting the very pronounced trends in the data. These effects include counterion condensation effects and deviations from non-free-draining (i.e., increased draining as the coil swells) measured by reduced viscosity and the strong interplay of intra- and interparticle interference effects in the light scattering.

This method should have numerous practical applications for optimizing product quality and process efficiency for a wide variety of modification reactions. For example, in this work targeted values of $[\eta]$ might be sought and controlled using ACOMP. On the other hand, the particular detectors used in this work did not allow a model-free measurement of the evolution of ξ, but this could be accomplished with FTIR or another more chemically sensitive detector.

At any rate, ACOMP is not restricted to postpolymerization conversion of neutral polymers to polyelectrolytes. Reactions that change mass or interactions with other polymers or small molecules can be followed, and chemically sensitive detectors can be added to the detector train to monitor changes in functional groups.

Acknowledgment. Support from NSF CTS 0623531, NASA NCC3-946, and La. BoR RD-B-7 is acknowledged. A. Paril acknowledges support from TUBITAK-BDP while visiting Tulane.

References and Notes

(1) Huisgen, R. In *1,3-Dipolar Cycloaddition Chemistry*; Padwa, A., Ed.; Wiley: New York, 1984; pp 1−176.
(2) Sumerlin, B. S.; Tsarevsky, N. V.; Louche, G.; Lee, R. Y.; Matyjaszewski, K. *Macromolecules* **2005**, *38*, 7540.
(3) Ladmiral, V.; Mantovani, G.; Clarkson, G. J.; Cauet, S.; Irwin, J. L.; Haddleton, D. M. *J. Am. Chem. Soc.* **2006**, *128*, 4823.
(4) Laurent, B. A.; Grayson, S. M. *J. Am. Chem. Soc.* **2006**, *128*, 4238.
(5) Florenzano, F. H.; Strelitzki, R.; Reed, W. F. *Macromolecules* **1998**, *31*, 7226.
(6) Giz, A.; Koc, A. O.; Giz, H.; Alb, A.; Reed, W. F. *Macromolecules* **2002**, *35*, 6557.
(7) Basu, S. *Nature (London)* **1951**, *168*, 341−342.
(8) Booth, F. *Proc. R. Soc. London, Ser. A* **1950**, *203*, 533−551.
(9) Drifford, M.; Dalbiez, J.-P. *J. Phys. Chem.* **1984**, *88*, 5368.
(10) Forster, S.; Schmidt, M. *Adv. Polym. Sci.* **1995**, *120*, 53.
(11) Li, X.; Reed, W. F. *J. Chem. Phys.* **1991**, *94*, 4568.
(12) Forster, S.; Schmidt, M.; Antonietti, M. *Polymer* **1990**, *31*, 781.
(13) Norwood, D. P.; Benmouna, M.; Reed, W. F. *Macromolecules* **1996**, *29*, 4293−4303.
(14) Sorci, G. A.; Reed, W. F. *Macromolecules* **2002**, *35*, 5218.
(15) Manning, G. S. *J. Chem. Phys.* **1969**, *51*, 1969.
(16) Reed, W. F.; Ghosh, S.; Medjahdi, G.; Francois, J. *Macromolecules* **1991**, *24*, 6189−6198.
(17) Schwartz, T.; Francois, J. *Makromol. Chem.* **1981**, *182*, 2757.
(18) Kulkarni, R. A.; Gundiah, S. *Makromol. Chem.* **1984**, *185*, 957.
(19) Zema, P.; Kowblansky, M. *Macromolecules* **1981**, *14*, 1451.
(20) Reed, C. E.; Reed, W. F. *J. Chem. Phys.* **1991**, *94*, 8479.
(21) Reed, W. F. In *Macroion, Characterization*; Schmitz, K., Ed.; *ACS Symp. Ser.* **1994**, *548*, 297−314.
(22) Odijk, T. *J. Polym. Sci., Phys.* **1977**, *15*, 477.
(23) Odijk, T.; Houwaart, A. C. *J. Polym. Sci., Phys.* **1978**, *16*, 627.
(24) Skolnick, J.; Fixman, M. *Macromolecules* **1977**, *10*, 9444.
(25) Reed, C. E.; Xiao, L.; Reed, W. F. *Biopolymers* **1989**, *28*, 1981.
(26) Kurata, M.; Yamakawa, H. *J. Chem. Phys.* **1958**, *29*, 311.
(27) It is noted that there is only a 4% change in $l_B = 0.708$ nm at 300 K (detector) to 0.737 nm at 333 K (reactor) since, for monovalent charge units, $l_B(m) = e^2/(4\pi\epsilon_0 D k_B T)$, where $D = 174.22 - 0.319T$ (K) is water's dielectric constant over T (K) $\in$ [273, 373].
(28) Muthukumar, M. *J. Chem. Phys.* **2004**, *120*, 9343.

MA070291X